Journal of Magnetism and Magnetic Materials 454 (2018) 356–361

Contents lists available at ScienceDirect

Journal of Magnetism and Magnetic Materials

journal homepage: www.elsevier.com/locate/jmmm

Research articles

Phase formation kinetics, hardness and magnetocaloric effect of sub-rapidly solidified $LaFe_{11.6}Si_{1.4}$ plates during isothermal annealing

Yuting Dai [a], Zhishuai Xu [b], Zhiping Luo [c], Ke Han [d], Qijie Zhai [b], Hongxing Zheng [a,b,*]

[a] Laboratory for Microstructures, Shanghai University, Shanghai 200444, China
[b] State Key Laboratory of Advanced Special Steel, Shanghai University, Shanghai 200444, China
[c] Department of Chemistry and Physics, Fayetteville State University, Fayetteville, NC 28301, USA
[d] National High Magnetic Field Laboratory, Florida State University, Tallahassee, FL 32310, USA

ARTICLE INFO

Article history:
Received 29 October 2017
Received in revised form 26 January 2018
Accepted 3 February 2018
Available online 5 February 2018

Keywords:
Magnetocaloric materials
La–Fe–Si
Phase transition
Centrifugal casting
Microstructure

ABSTRACT

High-temperature phase transition behavior and intrinsic brittleness of $NaZn_{13}$-type $\tau1$ phase in La–Fe–Si magnetocaloric materials are two key problems from the viewpoint of materials production and practical applications. In the present work, the Johnson-Mehl-Avrami-Kolmogorov (JMAK) equation was introduced to quantitatively characterize the formation kinetics of $\tau1$ phase in sub-rapidly solidified $LaFe_{11.6}Si_{1.4}$ plates during the isothermal annealing process. Avrami index was estimated to be 0.43 (~0.5), which suggests that the formation of $\tau1$ phase is in a diffusion-controlled one-dimensional growth mode. Meanwhile, it is found that the Vickers hardness as a function of annealing time for sub-rapidly solidified plates also agrees well with the JMAK equation. The Vickers hardness of $\tau1$ phase was estimated to be about 754. Under a magnetic field change of 30 kOe, the maximum magnetic entropy change was about 22.31 J/(kg·K) for plates annealed at 1323 K for 48 h, and the effective magnetic refrigeration capacity reached 191 J/kg.

1. Introduction

Solid-state magnetic refrigeration demonstrates a potential to replace the conventional vapor compression technology with its energy saving and environmentally benign features [1–3]. Several kinds of room-temperature magnetocaloric materials, including Gd–Si–Ge [4,5], Mn(As,Sb) [6], MnFe(P,As) [7], La–Fe–Si [8,9] and Heusler Ni–Mn–Ga(Sn,Sb) [10–13], have been explored. Among these materials, La–Fe–Si with an itinerant-electron metamagnetic (IEM) transition in cubic $NaZn_{13}$-type $La(Fe,Si)_{13}$ phase (denoted as $\tau1$ phase [14]) attracted tremendous attention due to low cost of raw materials and tunable Curie temperatures [15–20]. Presently, two key aspects should be addressed: (1) to clarify the high-temperature formation mechanism of the $\tau1$ phase for high-efficiency materials fabrication; and (2) to overcome the intrinsic brittleness of the $\tau1$ phase for high-frequency engineering applications.

It has been well accepted that the $\tau1$ phase in La–Fe–Si alloys with low Si concentration forms through a peritectic reaction ($\alpha(Fe) + L \rightarrow \tau1$) upon cooling [21–23]. However, narrow temperature window makes it difficult to obtain high-proportional $\tau1$ phase, and thus high-temperature annealing has to be conducted [24]. Up to date, the formation mechanism of $\tau1$ phase during annealing process is still unclear although a lot of efforts have been made [25–34]. Taking $LaFe_{11.6}Si_{1.4}$ bulk alloy as an example, Chen et al. [25] suggested that upon heating, the LaFeSi (1:1:1) phase first melts at 1407.6 K, and the $\tau1$ phase results from a peritectic reaction occurred between α(Fe) and liquid LaFeSi above this temperature; while below this temperature, a peritectoid reaction between α(Fe) and solid LaFeSi happens. In a different viewpoint, Fu et al. [26] proposed that an eutectoid reaction ($LaFeSi \rightarrow \tau1 + La_5Si_3$) could occur at 1402 K instead of the melting of LaFeSi phase; and Liu et al. [27] also speculated that the $\tau1$ phase may be associated with a certain eutectoid reaction based on the finding of lamellar microstructure when annealing $LaFe_{11.6}Si_{1.4}$ at 1323 K, and it should be noted that La_5Si_3 phase was invisible inside the lamellar transition layer although the eutectoid reaction was not specified.

Recently, we produced sub-rapidly solidified $LaFe_{11.6}Si_{1.4}$ plates (~2.5 mm thickness) with enhanced magnetocaloric properties using a centrifugal casting method. Compared with the conventional arc-melted bulk alloys, the formation of $\tau1$ phase in sub-rapidly solidified plates was strikingly facilitated, and a thermodynamic model has been proposed [35]. In order to optimize

* Corresponding author at: Laboratory for Microstructures, Shanghai University, Shanghai 200444, China.
E-mail address: hxzheng@shu.edu.cn (H. Zheng).

https://doi.org/10.1016/j.jmmm.2018.02.009
0304-8853/

heat-treatment routes, the Johnson-Mehl-Avrami-Kolmogorov (JMAK) equation will be introduced to characterize the formation kinetics of $\tau 1$ phase in sub-rapidly solidified $LaFe_{11.6}Si_{1.4}$ plates in the present work. On the other hand, only a limited literature was reported on the mechanical properties of La–Fe–Si magnetocaloric materials [36,37], so the JMAK equation will also be used to reveal the relationship between phase constituents and hardness so as to provide more information for practical applications.

2. Experimental

Pure La (99.9 wt%), Fe (99.99 wt%) and Si (99.999 wt%) were used to make sub-rapidly solidified $LaFe_{11.6}Si_{1.4}$ plates ($\sim$60 × 40 × 2.5 mm^3) by a centrifugal casting setup in argon under a cooling rate of $\sim$5000 K/s. Experimental details have been described elsewhere [35]. The produced plates were sealed in quartz tubes and annealed at 1323 K for various time durations, followed by water quenching. Three more experiments were performed at 1273 K for kinetic analysis of $\tau 1$ phase.

Microstructural observations were performed using a scanning electron microscope (SEM, JSM-6700) equipped with a backscatter image detector and an energy-dispersive spectrometer (Bruker EDS). The volume fractions of the phases were determined from the SEM images. The hardness measurements were performed by a Vickers hardness method using 500 gf load and 5 s of load duration (MVS-1000Z, China). The Vickers hardness was determined by averaging at least 10 readings. Topological morphology of intent was obtained by three-dimensional roughness reconstruction method. Magnetic properties were conducted on a physical property measurement system (Quantum Design PPMS-9) under a maximum magnetic field up to 30 kOe.

3. Results and discussion

3.1. Formation kinetics of $\tau 1$ phase

Backscattered SEM images revealed phase and microstructure in $LaFe_{11.6}Si_{1.4}$ plates (Fig. 1). Ultrafine and homogeneous microstructure was obtained throughout the as-cast plates (Fig. 1a), which consisted of black dendritic α(Fe) phase and white LaFeSi phase [35,38]. In the plate annealed at 1323 K for 3 h, $\tau 1$ phase emerged (Fig. 1b). With increased annealing time, more $\tau 1$ phase formed and consequently, both α(Fe) and LaFeSi phases decreased significantly (Fig. 1c–f). In the sample annealed for 48 h, the $\tau 1$ phase accounted for up to 94 vol%, while the α(Fe) and the LaFeSi phases each decreased to 3 vol%. The volume fractions of α(Fe), LaFeSi and $\tau 1$ phases as a function of the annealing time at 1323 K were presented in Fig. 2a. The evolution of phase and microstructure showed similar feature for those samples annealed at 1273 K (not shown here).

Previous researchers have shown that annealing of $LaFe_{11.6}Si_{1.4}$ bulk alloy at 1323 K for 300 h resulted in pure $\tau 1$ single phase [39]. Therefore the isothermal formation kinetics of $\tau 1$ phase can be described by the JMAK equation [40–46]

$$x(t) = 1 - \exp(-k_v t^n) \quad (1)$$

where $x(t)$ is the fraction of formation phase at the annealing time t; and where n (the Avrami index) and k_v (the formation rate constant) are two parameters characterizing the phase transition process. The value of k_v can be expressed by

$$k_v = k_0 \exp(-E/RT) \quad (2)$$

where k_0 is a constant, R is the gas constant, E is the activation energy, and T is the annealing temperature expressed in K. The

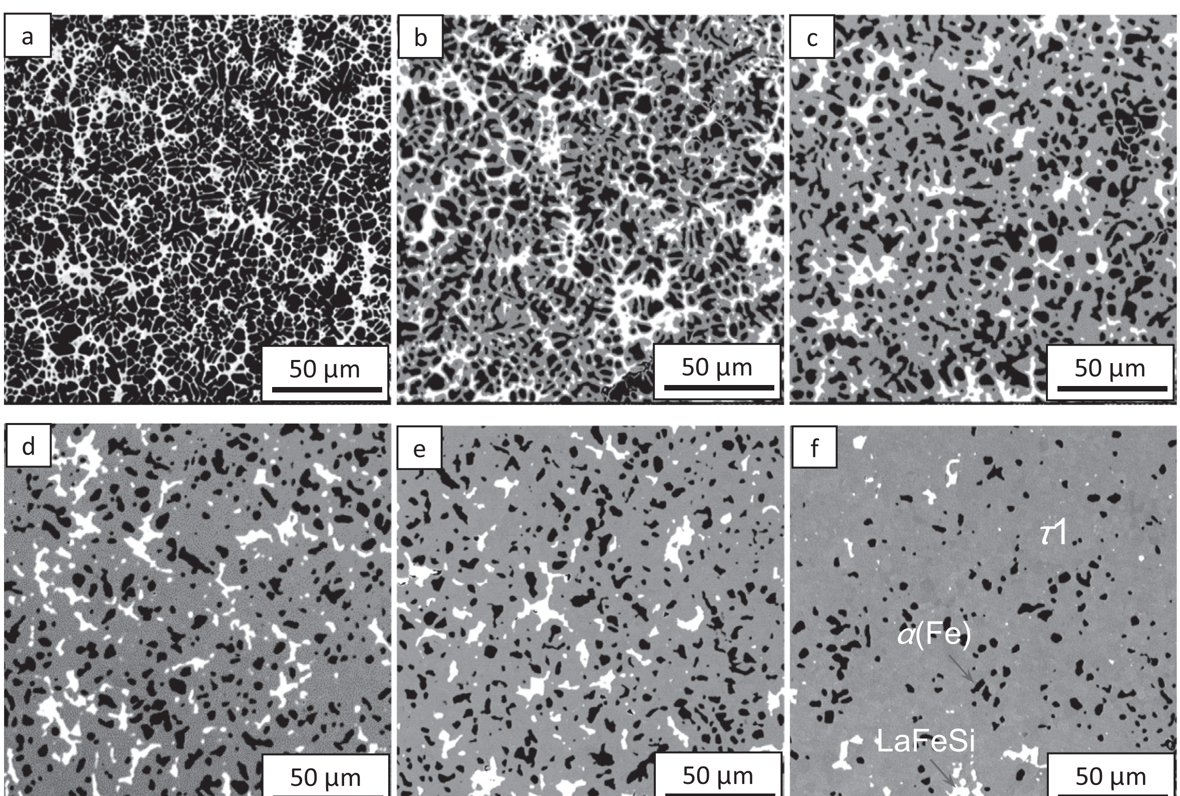

Fig. 1. Backscattered SEM images of $LaFe_{11.6}Si_{1.4}$ plates, as-cast state (a), annealed at 1323 K for 3 h (b), 6 h (c), 12 h (d), 24 h (e) and 48 h (f). The dark particles indicated by arrow are α(Fe) phase. The light particles indicated by arrows are from LaFeSi phase. The grey background is from $\tau 1$ phase.

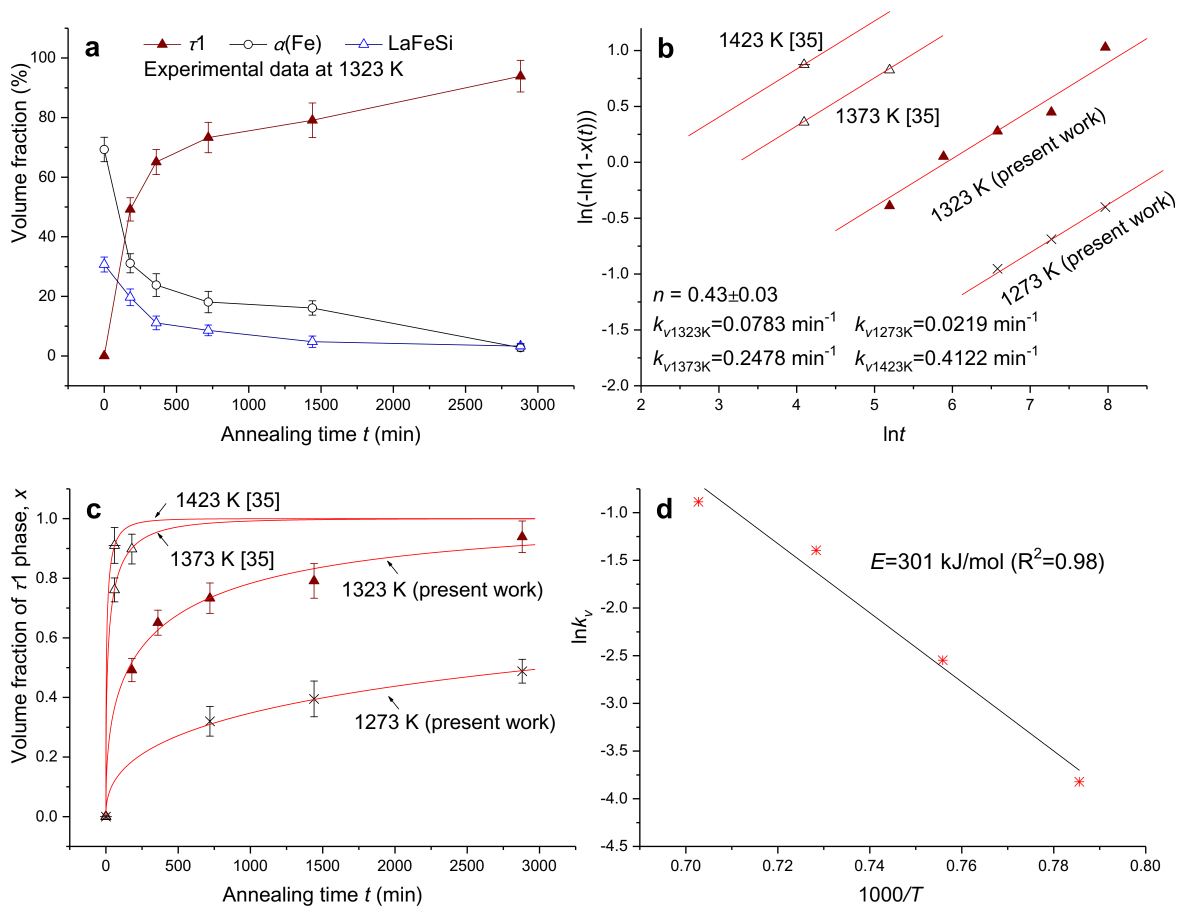

Fig. 2. (a) Volume fractions of α(Fe), LaFeSi and τ1 phases as a function of the annealing time at 1323 K. (b) $\ln(-\ln(1-x(t)))$ *vs.* ln*t* plot for the τ1 phase. (c) Formation rates of τ1 phase at 1323 K and 1273 K (present work), 1373 K and 1423 K [35], the solid lines indicating the fitting results from Eq. (1). (d) ln k_v *vs.* 1000/*T* plot.

Avrami index and formation rate constant can be evaluated from the slope and intercept from the plot of $\ln(-\ln(1-x(t)))$ against ln*t*, respectively, since Eq. (1) can also be written as follows:

$$\ln(-\ln(1-x(t))) = n\ln t + \ln k_v \tag{3}$$

For the formation of τ1 phase in sub-rapidly solidified $LaFe_{11.6}Si_{1.4}$ plates, our calculations showed that average value of n was 0.43 ± 0.03 for reactions occurring in the temperature range. The corresponding k values are listed in Fig. 2b. Fig. 2c presented the fitting results from Eq. (1). Using these four formation rates, the activation energy E for the formation of τ1 phase was estimated to be 301 kJ/mol (Fig. 2d), which is slightly lower than that in conventional arc-melted bulk alloys (∼312 kJ/mol [39]).

According to Table 1 [47], the n value of 0.43 in the sub-rapidly solidified plates suggests that the morphology of τ1 phase is close to thickening of very large plates with n = 0.5, which is a simplified model of continuous network growth of τ1 phase. The n can also be divided into three parameters: $n = a + b/c$, where a is the nucleation index; b is the dimensionality of growth; c is either 1 for linear or 2 for parabolic growth [48]. Because our data include only growth, a is zero. For a parabolic growth, c = 2. The b therefore should be 1, indicating a one-dimensional growth. While for the arc-melted bulk alloy with similar activation energy, n = 0.93 (∼1) [39] implies a two-dimensional thickening mechanism of discontinuous τ1 phase (b = 2) due to the initial coarse phase and microstructure.

Table 1
Summary of the n values in kinetic law $x(t) = 1 - \exp(-kt^n)$ during diffusion controlled growth process corresponding to various experimental conditions (from Ref. [47]).

	n
All shapes growing from small dimensions	≥1.5
Growth of particles of appreciable initial volume	1–1.5
Needles and plates of finite long dimensions	1
Thickening of long cylinders (needles)	1
Thickening of very large plates	0.5

3.2. Vickers hardness

The values of Vickers hardness for the samples annealed at 1323 K were given in Fig. 3a. During the isothermal process, the Vickers hardness increases with the volume fraction of the τ1 phase. We analyzed the Vickers hardness using the JMAK equation

$$H_e(t) = 1 - \exp(-k_{h\nu}t^m) \tag{4}$$

where $H_e(t)$ is defined as $H_e(t) = (H_t - H_0)/(H_\infty - H_0)$, H_0 is the hardness in the initial as-cast state, H_t is the hardness at annealing time t, H_∞ is the hardness at an infinitely long annealing time t_∞, k_{hv} is the temperature-dependent hardness rate constant, and m is the Avrami index. The estimated values of m and k_{hv} from our experimental data were 0.484 and 0.045 min^{-1}, respectively. Therefore, Vickers hardness as a function of annealing time at 1323 K can be expressed as

$$H_t = 754 - 540 \times \exp(-0.045 \times t^{0.484}) \tag{5}$$

As discussed above, one can conclude that the Vickers hardness of pure τ1 phase is about 754. Topological images of two typical indents showed that the indent becomes smaller after annealing

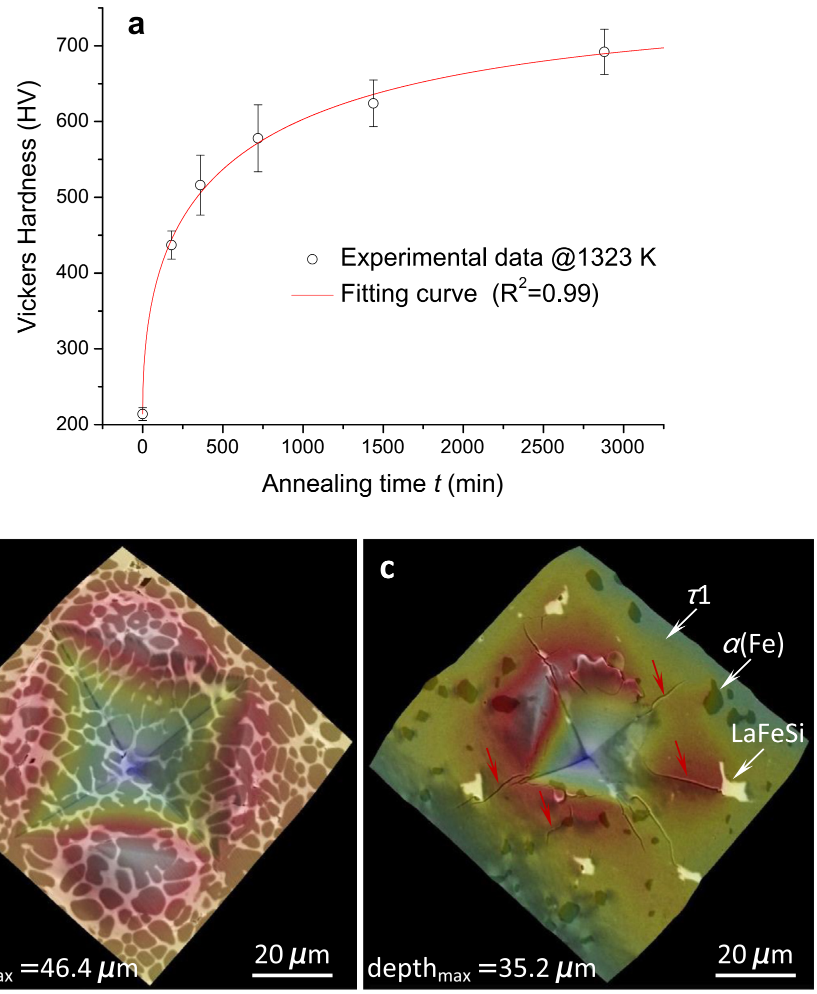

Fig. 3. (a) Vickers hardness as a function of the annealing time, the symbol and the solid line representing the experimental data and the fitting curve using Eq. (5), respectively. (b) Topological morphology of an indent in an as-cast sample; (c) Topological morphology in an annealed sample for 48 h. Cracks are marked by red arrows. Black and white contracts represent α(Fe) and LaFeSi, respectively. (For interpretation of the references to colour in this figure legend, the reader is referred to the web version of this article.)

for 48 h under the same load. In the as-cast sample (Fig. 3b), cracks were confined with the indented area. In the annealed sample (Fig. 3c), however, the crack extended to deformation-affected zone, and one can conclude that α(Fe) and LaFeSi phases are effective to hamper crack development to some extent.

3.3. Magnetocaloric properties

The present work investigated the magnetocaloric property of the $LaFe_{11.6}Si_{1.4}$ sample annealed for 48 h because it contained maximum volume fraction of τ1 phase among all samples. Magnetization curves (*M-T*) under a low magnetic field of 500 Oe were measured, which showed a ferromagnetic-paramagnetic IEM transition at about 189 K upon heating and a reverse transition at about 182 K upon cooling. To determine the Curie temperatures during heating and cooling processes, we assessed the minimum values of *dM/dT* for each of these curves (see inset in Fig. 4a). Isothermal magnetization curves (*M-H*) around the Curie temperature at intervals of 3 K between 150 K and 240 K show clear hysteresis losses between 186 K and 198 K (Fig. 4b). Arrot plots (M^2 *vs. H/M*) calculated for these isothermal magnetization curves show a typical S-shape around the Curie temperature (Fig. 4c), indicating that the annealed plate undergoes a first-order phase transition [49,50]. Using the Maxwell equation [51]

$$\Delta S_M(T,H) = \mu_0 \int_0^H \left(\frac{\partial M}{\partial T}\right)_H dH \tag{6}$$

The magnetic entropy change (ΔS_M) as a function of temperature can be calculated (Fig. 4d). The maximum $|\Delta S_M|$ values are 17.90 J/(kg·K), 21.24 J/(kg·K) and 22.31 J/(kg·K) under magnetic field changes of 10 kOe, 20 kOe and 30 kOe, respectively, which are higher than most reported values of $LaFe_{11.6}Si_{1.4}$ bulk alloys [28,52,53], and comparable to the values reported in $LaFe_{11.35}Co_{0.6}Si_{1.05}$ bulk alloy [54]. After subtracting the average hysteresis loss of 10.8 J/kg (inset in Fig. 4d), the effective refrigeration capacity (RC_{eff}) [55,56] reaches about 191 J/kg under a magnetic field change of 30 kOe.

4. Conclusions

(1) The JMAK equation was used to describe the formation kinetics of τ1 phase in sub-rapidly solidified $LaFe_{11.6}Si_{1.4}$ plates. The formation of τ1 phase is a diffusion-controlled one-dimensional growing process because of initial refined and homogeneous microstructure.
(2) The Vickers hardness of $LaFe_{11.6}Si_{1.4}$ annealed plates agrees well with the JMAK equation. The hardness of τ1 phase was estimated to be about 754.

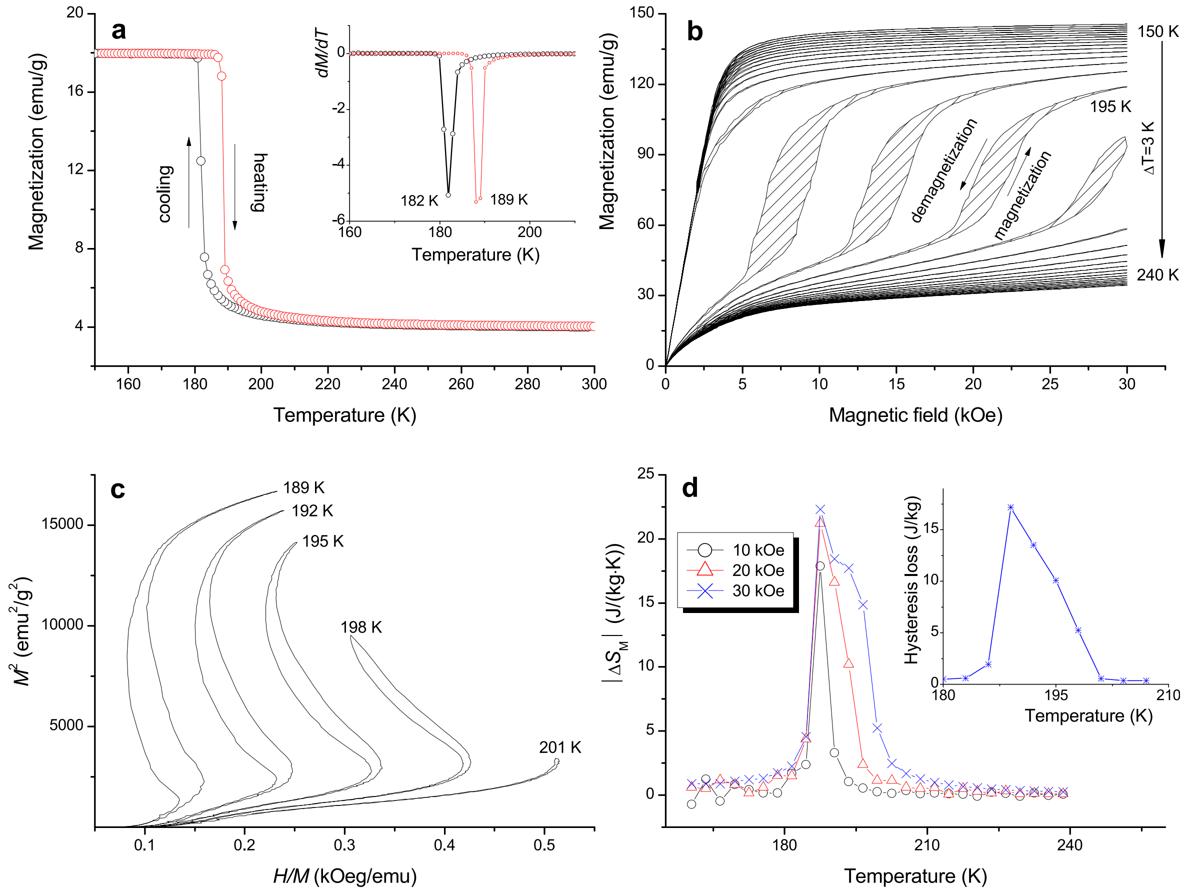

Fig. 4. (a) Magnetization curve (M-T) of $LaFe_{11.6}Si_{1.4}$ plate annealed for 48 h under a magnetic field of 500 Oe. The inset is the dM/dT plot showing the Curie temperatures. (b) Isothermal magnetization curves (M-H) measured between 150 K and 240 K under a magnetic field change of 30 kOe. Hysteresis losses between 186 K and 198 K are marked by stripped areas. (c) The Arrot plots (M^2 *vs.* H/M) around the Curie temperature. (d) Magnetic entropy change ($|\Delta S_M|$) values as a function of temperature, and the inset showing the hysteresis loss under 30 kOe.

(3) The sub-rapidly solidified $LaFe_{11.6}Si_{1.4}$ plate annealed at 1323 K for 48 h undergoes a first-order phase transition in the vicinity of 189 K upon heating, the maximum magnetic entropy change is 22.31 J/(kg·K) under a magnetic field change of 30 kOe, and the effective magnetic refrigeration capacity reaches 191 J/kg.

Acknowledgements

The authors gratefully acknowledge the financial support from the National Natural Science Foundation of China (51474144) and the Shanghai Sailing Program (17YF1405900). Part of the work was undertaken at the National High Magnetic Field Laboratory, which is supported by US NSF Cooperative Agreement (DMR–1157490) and the State of Florida. We thank Dr. Tyler for editing the manuscript.

Appendix A. Supplementary data

Supplementary data associated with this article can be found, in the online version, at https://doi.org/10.1016/j.jmmm.2018.02.009.

References

[1] M. Krautz, K. Skokov, T. Gottschall, C.S. Teixeira, A. Waske, J. Liu, System investigation of Mn substituted La(Fe, Si)$_{13}$ alloys and their hydrides for room-temperature magnetocaloric application, J. Alloys Compd. 598 (2014) 27–32.
[2] H. Fu, M. Zou, Q. Cao, V.K. Pecharsky, K.A. Gschneidner, L.S. Chumbely, Microstructure and magnetocaloric effects in partially amorphous $Gd_{55}Co_{15}Al_{30-x}Si_x$ alloys, Mater. Sci. Eng. A 528 (2011) 5219–5222.
[3] L. Zhang, S.C. Ma, Q. Ge, K. Liu, Q.Z. Jiang, X.Q. Han, S. Yang, K. Yu, Z.C. Zhong, A systematic study of the antiferromagnetic-ferromagnetic conversion and competition in MnNiGe: Fe ribbon systems, J. Mater. Sci. Technol. 33 (2017) 1362–1370.
[4] V.K. Pecharsky, K.A. Gschneidner Jr, Phase relationships and crystallography in the pseudobinary system Gd_5Si_4, J. Alloys Compd. 260 (1997) 98–106.
[5] K. Prabahar, D.M.R. Kumar, M.M. Raja, M. Palit, V. Chandrasekaran, Solidification behaviour and microstructural correlations in magnetocaloric Gd–Si–Ge–Nb alloys, Mater. Sci. Eng. B 172 (2010) 294–299.
[6] T. Morikawa, H. Wada, Effect of deviation from stoichiometry on magnetic and magnetocaloric properties in $MnAs_{1-x}Sb_x$, J. Magn. Magn. Mater. 272–276 (2004) 583–586.
[7] E. Bruck, O. Tegus, D.T.C. Thang, N.T. Trung, K.H.J. Buschow, A review on Mn based materials for magnetic refrigeration: Structure and properties, Int. J. Refrig. 31 (2008) 763–770.
[8] Q.Y. Dong, H.W. Zhang, T.Y. Zhao, J.R. Sun, B.G. Shen, Realization of a small hysteresis loss and large magnetic entropy change in $NaZn_{13}$-type La–Fe–Si compound, Solid State Commun. 147 (2008) 266–270.
[9] K. Niitsu, S. Fujieda, A. Fujita, R. Kainuma, Microstructure and magnetic properties of as-quenched cubic and tetragonal $La(Fe_{1-x}Si_x)_{13}$ compounds, J. Alloys Compd. 578 (2013) 220–227.
[10] V. Khovaylo, V. Koledov, V. Shavrov, M. Ohtsuka, H. Miki, T. Takagi, V. Novosad, Influence of cobalt on phase transition in $Ni_{50}Mn_{37}Sn_{13}$, Mater. Sci. Eng. A 481–482 (2008) 322–325.
[11] H.X. Zheng, W. Wang, S.C. Xue, Q.J. Zhai, J. Frenzel, Z.P. Luo, Composition-dependent crystal structure and martensitic transformation in Heusler Ni–Mn–Sn alloys, Acta Mater. 61 (2013) 4648–4656.
[12] O. Söderberg, I. Aaltio, Y. Ge, O. Heczko, S.-P. Hannula, Ni–Mn–Ga multifunctional compounds, Mater. Sci. Eng. A 481–482 (2008) 80–85.
[13] H.S. Akkera, N. Choudhary, D. Kaur, Martensitic phase transformations and magnetocaloric effect in Al co-sputtered Ni–Mn–Sb alloy thin films, Mater. Sci. Eng. B 198 (2015) 113–119.
[14] V. Raghavan, Fe–La–Si (iron–lanthanum–silicon), J. Phase Equilib. 22 (2001) 158–159.

[15] E.Y. Zhang, Y.G. Chen, Y.B. Tang, Investigation on corrosion and galvanic in $LaFe_{11.6}Si_{1.4}$ alloy, Mater. Chem. Phys. 127 (2011) 1–6.
[16] M. Zhang, Y. Long, R.C. Ye, Y.Q. Chang, Corrosion behavior of magnetic refrigeration material La–Fe–Co–Si in distilled water, J. Alloys Compd. 509 (2011) 3627–3631.
[17] H. Zhang, B.G. Shen, Z.Y. Xu, X.Q. Zheng, J. Shen, F.X. Hu, J.R. Sun, Y. Long, Reduction of hysteresis loss and large magnetocaloric effect in C- and H-doped $La(Fe, Si)_{13}$ compounds around room temperature, J. Appl. Phys. 111 (2012) 07A909.
[18] H. Yamada, K. Fukamichi, T. Goto, Recent advances of itinerant-electron metamagnetism and related properties of intermetallic compounds, Phys. B: Condens. Matter 327 (2003) 148–154.
[19] J. Sun, Y.X. Li, Q.Y. Dong, J.R. Sun, Magnetocaloric properties of the $La_{0.7}Pr_{0.3}Fe_{13-x}Si_x$ compounds, J. Magn. Magn. Mater. 321 (2009) 2336–2339.
[20] H. Zhang, Y. Long, M. Zou, K.A. Gschneidner Jr, V.K. Pecharsky, Effect of Ca on the microstructure and magnetocaloric effects in the $La_{1-x}Ca_xFe_{11.5}Si_{1.5}$ compounds, J. Alloys Compd. 509 (2011) 3746–3750.
[21] J.J. Ipus, J.M. Borrego, L.M. Moreno-Ramírez, J.S. Blázquez, V. Franco, A. Conde, Grinding and particle size selection as a procedure to enhance the magnetocaloric response of $La(Fe, Si)_{13}$ bulk samples, Intermetallics 84 (2017) 30–34.
[22] S.T. Feng, Y. Fang, Q.J. Zhai, Z.P. Luo, H.X. Zheng, Magnetocaloric effect in a dual-phase coupled $LaFe_{11}Si_2$ crystal prepared by a modified high-pressure zone-melting technique, J. Cryst. Growth 45 (2016) 83–87.
[23] J. Liu, C. He, M.X. Zhang, A.R. Yan, A systematic study of the microstructure, phase formation and magnetocaloric properties in off-stoichiometric La–Fe–Si alloys, Acta Mater. 118 (2016) 44–53.
[24] K. Niitsu, R. Kainuma, Phase equilibria in the Fe–La–Si ternary system, Intermetallics 20 (2012) 160–169.
[25] X. Chen, Y.G. Chen, Y.B. Tang, High-temperature phase transition and magnetic property of $LaFe_{11.6}Si_{1.4}$ compound, J. Alloys Compd. 509 (2011) 8534–8541.
[26] S. Fu, Y. Long, Y.Y. Sun, J. Hu, Microstructure evolution and phase transition dependent on annealing temperature and carbon content for $LaFe_{11.5}Si_{1.5}C_x$ compounds prepared by arc-melting, Intermetallics 39 (2013) 79–83.
[27] J. Liu, M. Krautz, K. Skokov, T.G. Woodcock, O. Gutfleisch, Systematic study of the microstructure, entropy change and adiabatic temperature change in optimized La–Fe–Si alloys, Acta Mater. 59 (2011) 3602–3611.
[28] T. Liu, Y.G. Chen, Y.B. Tang, S.F. Xiao, E.Y. Zhang, J.W. Wang, Structure and magnetic properties of shortly high temperature annealing $LaFe_{11.6}Si_{1.4}$ compound, J. Alloys Compd. 475 (2009) 672–675.
[29] M.X. Zhang, J. Liu, C. He, A.R. Yan, Novel microstructure and large magnetocaloric effect in $La_2Fe_{11}Si_2$ magnetic refrigerant, Mater. Lett. 134 (2014) 87–90.
[30] M.X. Zhang, J. Liu, Y. Zhang, J.D. Dong, A.R. Yan, K.P. Skokov, O. Gutfleisch, Large entropy change, adiabatic temperature change, and small hysteresis in $La(Fe, Mn)_{11.6}Si_{1.4}$ strip-cast flake, J. Magn. Magn. Mater. 377 (2015) 90–94.
[31] S.H. Xie, J.Q. Li, Y.H. Zhuang, Influence of boron on the giant magnetocaloric effect of $La(Fe_{0.9}Si_{0.1})_{13}$, J. Magn. Magn. Mater. 311 (2007) 589–593.
[32] M. Balli, D. Fruchart, O. Sari, J.H. Huang, M. Rosca, Refrigerant capacity and direct measurements of the magnetocaloric effect on $LaFe_{11.2}Co_{0.7}Si_{1.1}C_x$ materials, J. Appl. Phys. 107 (2010) 09A933.
[33] X.C. Zhong, X.L. Feng, X.W. Huang, X.Y. Shen, Z.W. Liu, Structure and magnetocaloric effect of $La_{0.7}Ce_{0.3}(Fe_{0.92}Co_{0.08})_{11.4}Si_{1.6}$ bulk alloy prepared by powder metallurgy, J. Alloys Compd. 685 (2016) 913–916.
[34] A.S. Demuner, A.Y. Takeuchi, E.C. Passamani, J.R. Proveti, C. Larica, E. Favre-Nicolin, A.M. Gomes, Magnetocaloric properties of $(La-Gd)Fe_{11.4}Si_{1.6}$ metamagnetic compound, J. Magn. Magn. Mater. 321 (2009) 1809–1813.
[35] Z.S. Xu, Y.T. Dai, Y. Fang, Z.P. Luo, K. Han, C.J. Song, Q.J. Zhai, H.X. Zheng, High-temperature phase transition behavior and magnetocaloric effect in a sub-rapidly solidified La–Fe–Si plate produced by centrifugal casting, J. Mater. Sci. Technol. (2017), https://doi.org/10.1016/j.jmst.2017.11.023.
[36] Y.Y. Shao, J. Liu, M.X. Zhang, A.R. Yan, K.P. Skokov, D. Yu Karpenkov, O. Gutfleisch, High-performance solid-state cooling materials: balancing magnetocaloric and non-magnetic properties in dual phase La–Fe–Si, Acta Mater. 125 (2017) 506–512.
[37] B. Kaeswurn, A. Barcza, M. Vögler, P.T. Geiger, M. Katter, O. Gutfleisch, L.F. Cohen, Behaviour of the Young's modulus at the magnetocaloric transition in $La(Fe,Co,Si)_{13}$, J. Alloys Compd. 697 (2017) 427–433.
[38] P. Gębara, P. Pawlik, E. Kulej, J.J. Wyslocki, K. Pawlik, A. Przybył, The evolution of microstructure in annealed LaFeSi-type alloys, Opt. Appl. 39 (2009) 761–764.
[39] S. Fujieda, K. Fukamichi, S. Suzuki, Microstructure and isothermal magnetic entropy change of $La(Fe_{0.89}Si_{0.11})_{13}$ in a single-phase formation process by annealing, J. Alloys Compd. 56 (2013) 196–200.
[40] W.A. Johnson, R.F. Mehl, Reaction kinetics in processes of nucleation and growth, Trans. AIME 135 (1939) 416–458.
[41] M. Avrami, Kinetics of phase change. I general theory, J. Phys. Chem. 7 (1939) 1103.
[42] M. Avrami, Kinetics of phase change: II. Transformation-time relations for random distribution of nuclei, J. Chem. Phys. 8 (1940) 212–224.
[43] A.N. Kolmogorov, On the statistical theory of crystallization of metals, Bull. Acad. Sci. USSR Math. Ser 1 (1937) 355–359.
[44] A. Fujita, H. Yako, Kinetics of thermal induced first-order magnetic transition in $La(Fe_{0.88}Si_{0.12})_{13}$ itinerant electron metamagnet, J. Alloys Compd. 577S (2013) S48–S51.
[45] H. Yako, S. Fujieda, A. Fujita, K. Fukamichi, Influence of demagnetization effect on the kinetics of the itinerant electron metamagnetic transition in magnetic refrigerant, IEEE Magn. Trans. 47 (2011) 2482–2485.
[46] J. Málek, The applicability of Johnson-Mehl-Avrami model in the thermal analysis of the crystallization kinetics of glasses, Thermochim. Acta 267 (1995) 61–73.
[47] J.W. Christain, The Theory of Transformations in Metals and Alloys I: Equilibrium and General Kinetic Theory, Pergamon Press, Oxford, 1975.
[48] S. Ranganathan, M. Von Heimendahl, The three activation energies with isothermal transformations: applications to metallic glasses, J. Mater. Sci. 16 (1981) 2401–2404.
[49] A. Fujita, Y. Akamatsu, K. Fukamichi, Itinerant electron metamagnetic transition in $La(Fe_xSi_{1-x})_{13}$ intermetallic compounds, J. Appl. Phys. 85 (1999) 4756.
[50] J. Inoue, M. Shimizu, Volume dependence of the first-order transition temperature for RCo_2 compounds, J. Phys. F: Metal Phys. 12 (1982) 1811.
[51] D.Z. Wu, S.C. Xue, J. Frenzel, G. Eggeler, Q.J. Zhai, H.X. Zheng, Atomic ordering effect in $Ni_{50}Mn_{37}Sn_{13}$ magnetocaloric ribbons, Mater. Sci. Eng. A 534 (2012) 568–572.
[52] P.N. Zhang, J. Liu, Y.Y. Shao, A.R. Yan, Direct formation of $NaZn_{13}$-structure $La(Fe, Si)_{13}$ phase by directional solidification, Mater. Lett. 193 (2017) 34–37.
[53] B.G. Shen, J.R. Sun, F.X. Hu, H.W. Wang, Z.H. Cheng, Recent progress in exploring magnetocaloric materials, Adv. Mater. 21 (2009) 4545–4564.
[54] P. Gębara, Magnetocaloric effect of $LaFe_{11.35}Co_{0.6}Si_{1.05}$ alloy, Rare Met. (2017), https://doi.org/10.1007/s12598-017-0917-6.
[55] A.O. Pecharsky, K.A. Gschneidner Jr., V.K. Pecharsky, The giant magnetocaloric effect of optimally prepared $Gd_5Si_2Ge_2$, J. Appl. Phys. 93 (2003) 4722–4728.
[56] I. Radelytskyi, M. Pękała, R. Szymczak, D.J. Gawryluk, M. Berkowski, J. Fink-Finowicki, R. Diduszko, V. Dyakonov, H. Szymczak, Magnetocaloric effect in Ni_2MnGa single crystal in the vicinity of the martensitic phase transition, J. Magn. Magn. Mater. 430 (2017) 16–21.